Identification of an SH3-Binding Motif in a New Class of Methionine Aminopeptidases from *Mycobacterium tuberculosis* Suggests a Mode of Interaction with the Ribosome[†,‡]

Anthony Addlagatta,[§] Michael L. Quillin,[§] Omonike Omotoso,[||] Jun O. Liu,[||] and Brian W. Matthews*[,§]

Institute of Molecular Biology, Howard Hughes Medical Institute and Department of Physics, 1229 University of Oregon, Eugene, Oregon 97403-1229, and Department of Pharmacology and Molecular Sciences, Johns Hopkins School of Medicine, 725 North Wolfe Street, Baltimore, Maryland 21205

Received January 20, 2005; Revised Manuscript Received March 25, 2005

ABSTRACT: The crystal structure of the methionine aminopeptidase (MetAP) from *Mycobacterium tuberculosis* (MtMetAP1c) has been determined in the apo- and methionine-bound forms. This is the first structure of a type I MetAP with a significant extension at the amino terminus. The catalytic domain is similar to that of *Escherichia coli* MetAP (EcMetAP), and the additional 40-residue segment wraps around the surface with an extended but well-defined structure. There are several members of the actinomyces family of bacteria that contain MetAPs with such N-terminal extensions, and we classify these as MetAP type Ic (MetAP1c). Some members of this family of bacteria also contain a second MetAP (type Ia) similar in size to EcMetAP. The main difference between the apo- and the methionine-bound forms of MtMetAP1c is in the conformation of the metal-binding residues. The position of the methionine bound in the active site is very similar to that found in many of the known members of this family. Side chains of several residues in the S1 and S1′ subsites shift as much as 1.5 Å compared to EcMetAP. Residues 14−17 have the sequence Pro-Thr-Arg-Pro and adopt the conformation of a polyproline II helix. Model-building suggests that this PxxP segment can bind to an SH3 protein motif. Other type Ib and type Ic MetAPs with N-terminal extensions contain similarly located PxxP motifs. Also, several ribosomal proteins are known to include SH3 domains, one of which is located close to the tunnel from which the nascent polypeptide chain exits the ribosome. Therefore, it is proposed that the binding of MetAPs to the ribosome is mediated by a complex between a PxxP motif on the protein and an SH3 domain on the ribosome. It is also possible that zinc-finger domains, which are located at the extreme N-terminus of type I MetAPs, may participate in interactions with the ribosome.

Many proteins undergo post-translational modification, one of the most common forms being the removal of the initiator methionine by methionine aminopeptidases (MetAP) (*1*). The N-terminal methionine of nascent polypeptide chains is cotranslationally removed, and the efficiency of cleavage depends in large part on the size of the side chain of the penultimate residue.

MetAPs are classified as type I and type II, the latter having a 60-amino acid insertion within the catalytic domain. Eubacteria contain only type I MetAPs; archea have type II enzymes, and eukaryotes contain both (*1*, *2*). Type I enzymes have traditionally been further subdivided into type Ia and type Ib (Figure 1), depending on the presence or absence of an N-terminal extension. Type Ia enzymes contain only the catalytic domain, with the prototypical example being

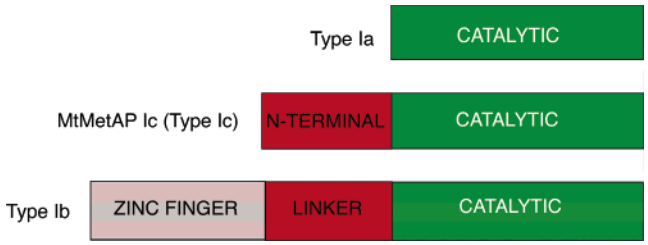

FIGURE 1: Domain architecture of type I MetAPs. The catalytic domain (green) is present in all MetAPs; however, in the type Ib enzymes, this domain is preceded by a zinc-finger domain (gray) and a linker (red). *Mycobacterium tuberculosis* (MtMetAP1c) has an extension at the N-terminus, homologous to the linker, but lacks the zinc-finger domain. It is here classified as a type Ic MetAP.

Escherichia coli MetAP (EcMetAP). Type Ib enzymes have an N-terminal extension of about 120 amino acids which includes two zinc-fingers and a 50-amino acid linker to the catalytic domain (Figure 1). These include enzymes from yeast (ScMetAP1) and human (HsMetAP1). Limited proteolysis of the yeast type Ib MetAP suggested that the two zinc fingers are in one domain and the linker and catalytic domain in another (*3*). Recently, a third form of the type I enzyme was found represented by a MetAP from mycobacteria; it contains a relatively short N-terminal extension

[†] This work was supported in part by NIH Grant GM20066 (B.W.M.). Financial support from the Keck Center (J.O.L.) is also gratefully acknowledged.

[‡] Coordinates have been deposited in the Protein Data Bank (access codes 1Y1N and 1YJ3).

* To whom correspondence should be addressed. Phone: (541) 346-2572. Fax: (541) 346-5870. E-mail: brian@uoxray.uoregon.edu.

[§] University of Oregon.

[||] Johns Hopkins School of Medicine.

10.1021/bi0501176 CCC: $30.25
Published on Web 04/21/2005

that lacks the two zinc finger motifs in mammalian MetAP1b (*4*). As discussed below, we propose that MetAPs with a shorter N-terminal extension (~40 amino acids) be classified as type Ic enzymes.

Deletion of the lone MetAP gene from prokaryotes, or both MetAPs from yeast, is lethal (*5*, *6*). Consequently, MetAPs are recognized as drug targets for treating microbial and fungal infections. The type II enzyme in eukaryotes has also been identified as a target for the antiangiogenic compounds fumagillin, ovalicin, and TNP-470 for treating cancers (*7*−*9*). Several crystal structures have been reported for the prokaryotic MetAPs and their complexes with different inhibitors (*10*−*14*).

Mycobacterium tuberculosis causes the highest annual global mortality of all known pathogens (*15*). The rise in tuberculosis (TB) incidence over the last two decades is partly due to TB deaths among HIV-infected patients and partly due to the emergence of multidrug resistant strains of the bacteria (*16*). These resistant strains are alarming for two reasons. First, there are only a few effective drugs available to treat TB infection, and drug-resistant strains could give rise to a potentially untreatable form of the disease. Second, although only 5% of immunocompetent people infected with *M. tuberculosis* succumb to the disease, it is nevertheless highly contagious (*17*). Therefore, new targets and inhibitors for TB treatment are needed. The MtMetAPs have less than 48% sequence identity with their human counterpart, HsMetAP1, suggesting that it may be possible to find inhibitors that are selective against the bacterial enzyme.

Two isoforms of MetAPs have been identified in *M. tuberculosis*, one with size similar to EcMetAP (type Ia) and the second with an N-terminal extension of about 40 amino acids (MtMetAP1c). To understand the structural role of the N-terminal extension in MetAPs, we have determined the X-ray crystal structure of the apo- and methionine-bound forms of MtMetAP1c. All the residues that coordinate the metal ions and most of the residues that make up the S1 and S1′ sites are highly conserved in sequence and in structure with other MetAPs. The N-terminal extension is proline-rich and has sequence homology with the linker region of the type Ib enzymes including human MetAP1 (Figure 1). This extension lies across the surface of the catalytic domain and includes an exposed Pro-x-x-Pro (PxxP) motif that appears poised to bind to a Src-homology 3 (SH3) domain. This suggests that MetAP1s might bind to ribosomes via a PxxP motif within their linker region that is recognized by an SH3 domain within the ribosome.

MATERIALS AND METHODS

Protein Purification. DNA encoding MtMetAP1c was amplified from microbacterial genomic DNA kindly provided by William Bishai (Johns Hopkins School of Medicine) using the following primer pair: 5′-primer, 5′-GCGGGATC-CCCTAGTCGTACCGCGCTC-3′; 3′-primer, 5′-GCGCTC-GAGCTACAGACAGGTCAGGATC-3′. MtMetAP1c was subcloned into a pET28a vector encoding an N-terminal poly-His-tag to give pET-MtMetAP1c, which was confirmed by sequencing. pET-MtMetAP1c was then transformed into *E. coli* [BL21 (DE3), Stratagene]. Two liters of LB media with 100 mL of overnight culture was incubated at 37 °C until an OD_{600} of 1.2 was achieved. The culture was induced with 1 mM (final concentration) IPTG for 12 h. Cells were harvested and resuspended in 100 mL of +T/G buffer (50 mM Hepes, pH 8.0, 0.5 M KCl, 10% glycerol, 0.1% Triton-X 100, and 5 mM imidazole) and were passed through a French press twice and centrifuged at 18 000*g* for 20 min. The supernatant was passed through a +T/G preequilibrated metal affinity column (talon resin, Clontech), and the column was washed with the same buffer followed by −T/G buffer (50 mM Hepes, pH 8.0, 0.5 M KCl, and 5 mM imidazole). The protein was eluted by 100 mM imidazole in −T/G into a flask with 1 mL of 0.5 M EDTA (pH 8.0) and was dialyzed into a buffer containing 25 mM Hepes, pH 8.0, 0.5 M KCl, and 5 mM methionine. After concentration, the protein was loaded onto a Superdex 75 Hi-load prep-grade 16/60 gel filtration column (Pharmacia) equilibrated with 25 mM Hepes, pH 6.8, 25 mM K_2SO_4, and 150 mM NaCl. No attempts were made to remove the N-terminal His-tag. Protein concentration was determined by absorption at 280 nm using an extinction coefficient of 1.273 $M^{-1}\cdot cm^{-1}$. Final yield of the protein was about 300 mg for 2 L of culture.

Crystallization and Data Collection. Crystals of MtMetAP1c were grown by the vapor diffusion method at 25 °C. Hanging drops at room temperature contained 5 μL of protein solution (10 mg/mL) and 5 μL of well solution consisting of 26−28% PEG 2000 monomethyl ether, 100 mM 2,2-bis-(hydroxymethyl)-2,2′,2″-nitrilotriethanol, pH 6.5, and 1−2 mM oxidized β-mercaptoethanol. Thin platelike crystals appeared in 24 h. Crystals were transferred into a stabilizing solution of 26−28% PEG 2000 monomethyl ether and 100 mM 2,2-bis(hydroxymethyl)-2,2′,2″-nitrilotriethanol (pH 6.5) for further modification. Freshly prepared $CoCl_2$ (1−2 mM) followed by 1−2 mM methionine was added to some crystals.

Crystals were frozen in a stream of nitrogen gas at 100 K without any extra cryo-protectant. X-ray diffraction data were collected at 100 K on an R-axis IV with a Rigaku rotating anode source for the Met structure. For the apo-structure, the synchrotron X-ray source at the Advanced Light Source (ALS, Berkeley, CA) on beamline 8.2.2 was used. Data were processed by HKL2000 and Scalepack (*18*). The structure was solved by molecular replacement (*19*) based on the structure (*10*) of *E. coli* MetAP (PDB entry 1C21). Refinement and model-building were done in CNS and O, respectively (*20*, *21*). The N-terminal extension was traced in several steps during refinement of the methionine-bound structure. The final coordinates of the complex with methionine were used to solve the apo-structure. Data processing and refinement statistics are summarized in Table 1.

Modeling and Sequence Alignment. To compare and align sequences, the clustalW and Alscript programs were used (*22*, *23*). Three-dimensional structures were compared with LSQMAN (*24*). Figures were prepared with Molscript5 (*25*) and PyMOL (*26*).

RESULTS AND DISCUSSION

Overall Structure. This is the first structure determination of a MetAP with an N-terminal extension similar to the type Ib enzymes. Except for the first three residues, the entire protein could be modeled into electron density. The catalytic domain has a pita-bread fold similar to that observed in other

Table 1: X-ray Data Collection and Refinement Statistics[a]

	apo-structure	complex with Co^{2+} and Met
Cell Parameters		
space group	$P2_1$	$P2_1$
a (Å)	49.34	49.36
b (Å)	47.91	48.16
c (Å)	56.82	56.54
β(deg)	95.11	95.05
X-ray Data Collection		
wavelength (Å)	0.977	1.5418
resolution range (Å)	20−1.51 (1.56−1.51)	20−1.6 (1.66−1.6)
collected reflections	1 108 529	365 285
unique reflections	41 425 (4038)	33 032 (2979)
completeness (%)	99.5 (97.1)	94.2 (85.8)
$\langle I/\sigma(I)\rangle$	30.7 (7.7)	10.5 (1.8)
R_{sym} (%)	4.6 (16.4)	8.0 (30.0)
Refinement Statistics		
R (%)	20.2	20.7
R_{free} (%)	24.7	25.4
Δ_{bonds} (Å)	0.02	0.02
Δ_{angles} (deg)	2.2	1.9

[a] Numbers given in parentheses correspond to the highest-resolution shell of data.

members of the family with the extra residues of the amino-terminus wrapping around this domain (Figure 2). Two cobalt ions and a methionine were modeled in the Met structure. All of the residues that normally contact the metal ions are conserved. MtMetAP1c is shorter by eight amino acids at the C-terminus compared to EcMetAP. Diffuse electron density suggested that Cys285 in the Met structure had been modified by β-mercaptoethanol. An apparent potassium ion was identified about 13 Å away from the active site, similar to the cation seen in EcMetAP (*8*).

A New Class of MetAPs with a Shorter N-Terminal Extension. Several MetAPs with an extension similar to that in the present structure have been identified from a BLAST (*27*) search of the Swiss-prot/Tremble database (*4*) (Figure 3). These have sequence identity higher than 42% in the N-terminal extension. All these species are high-GC content, gram-positive bacteria, classified as actinomycetes. No other bacterial species whose sequence has been determined has such an N-terminal extension. These MetAPs are not accurately represented by either the MetAP1a or MetAP1b family. Therefore, we propose that they be classified as MetAP type Ic (MetAP1c). A BLAST search with the *M. tuberculosis* MetAP without the extension indicated that several of these species have a second MetAP close in size to EcMetAP.

Structure of the N-Terminal Extension. The 40-amino acid extension at the N-terminus wraps around the surface of the catalytic domain in a contiguous crevice (Figure 2) and makes extensive sequence-specific contacts (Figure 4). There are no secondary structural elements in the N-terminal extension. The side chain of Arg4 forms a salt bridge with Asp126 which stabilizes the N-terminal end. While some of the residues on the catalytic domain that interact with the N-terminal extension in MtMetAP1c are the same as in EcMetAP [Glu110 (MtMetAP1c)/75 (EcMetAP), Asp118/83, Lys102/67, Asp78/42, Tyr97/62], the others are not [Ser119/Asp84 and Ala85 (insertion of an aa), Asp75/Gly39, His82/Asn46, Thr210/Gly176, Ser93/Ala58, Trp251/Met217, Tyr91/Val56, Gly89/His54, Tyr135/Ile101, Val210/Gly176]. Residues which are conserved adopt slightly different conformations to accommodate the new partners. Truncation of the N-terminal extension could render the hydrophobic residues solvent-exposed and thereby destabilize the protein as seen in studies of the Δ1−135 mutant of HuMetAP1 (*28*). Electrostatic surface potential calculations of MtMetAP1c with and without the N-terminal extension indicate that the crevice on the catalytic domain has both hydrophobic and hydrophilic regions (Figure 4a).

Methionine-Bound Structure. Clear density was observed for two cobalt ions and the methionine in the active site. Overlay of the structure on EcMetAP (PDB: 1C21) showed a rmsd of 0.95 Å for all the C^{α} atoms (Figure 5a). The methionine side chain is buried in a hydrophobic pocket formed by several conserved residues (Figure 5b). The position of the methionine is in a similar orientation as in other MetAP structures. The amino group interacts with Co2, and one of the oxygen atoms of the carboxylate forms a bridge between the two cobalt ions (1.9 Å with Co1 and 2.1 Å with Co2), while the other forms a hydrogen bond with His114 (2.8 Å) that is conserved in other MetAP1s (His79 in EcMetAP).

Some changes were observed in the side chains of the residues in the S1 and S1′ sites compared to those in the EcMetAP structure (PDB entry 1C21). Residues in the hydrophobic S1 pocket are conserved between EcMetAP and MtMetAP1c, except for Thr94 and Phe100 in place of Cys59 and Tyr65 in EcMetAP. Among conserved residues, slight structural changes are evident. For example, Trp255 (Trp221 in EcMetAP) shifts by 1.5 Å, Phe202 (Tyr168) by 1.1 Å, and His114 (His79) by 1.0 Å. The side chain of His212 (His178) rotates around $C^{\alpha}-C^{\beta}$ by about 15° into the substrate-binding tunnel (Figure 5b). It was reported that full-length and the Δ1−66 mutant of HuMetAP1 (which still has the linker region) have a similar affinity for methionine, but the Δ1−135 mutant loses specificity and can accommodate residues as large as phenylalanine and isoleucine (*28*). These observations suggest that the N-terminal extensions in MetAPs modulate and help define the specificity of the active site. Given that the active sites of all the MetAPs are highly conserved, which poses a challenge in designing inhibitors specific for a given MetAP, the differences in the positions in the S1 and S1′ residues, although small, could be useful to differentiate between MetAPs with and without an N-terminal extension.

Structure of the Apoenzyme. The rms deviation in the positions of C^{α} atoms between the apo- and Met-forms is only 0.19 Å, showing that there are no major structural changes in the protein structure upon binding either methionine or metal ions. As expected, the maximum difference is seen in the conformation of the residues that bind to the metal ions (Figure 6). There is no density in the active site that would suggest the presence of any metal ions including those used in the crystallization buffer such as sodium and potassium. The average thermal parameters of the carboxylate oxygen atoms of the ligands Asp131, Asp142, Glu238, and Glu269 in the cobalt-bound structure (8.7 $Å^2$) are much lower than in the apo-structure (17.2 $Å^2$), suggesting that these residues are more mobile in the latter. Several apparent hydrogen-bonding contacts between the O-atoms of these carboxylates suggest some degree of protonation for these residues in the absence of metals.

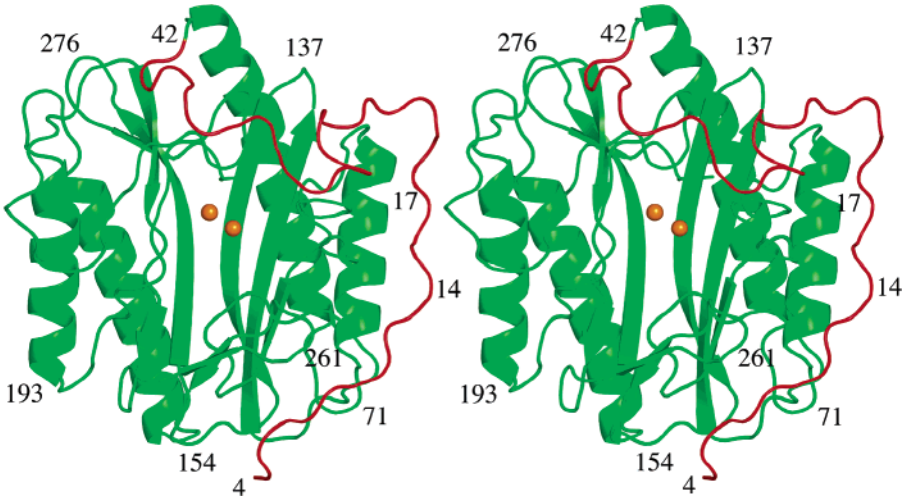

FIGURE 2: Stereo drawing showing the structure of *Mycobacterium tuberculosis* methionine aminopeptidase. The N-terminal extension (shown in red) makes close contact with the catalytic domain (shown in green). The PxxP motif comprises residues 14−17.

1		MPS--RTALSPGVLSPTRPVPNWIARPEYVGKPAAQEGS-EPW	(40)
2		MPKDSTGHLIPGRVSASRPVPSHIPQPEYVGKAGPAP-SDRGD	(42)
3	(2)	TPKNAYGHLVPGDISAARWVDPKIARPNYVGKKRVPR-YTGSD	(42)
4		-----MSAIKPYPQSPRRHVPGNIARPPYVGLGDVPETYDGSH	(37)
5		--MSGQSLLVPGELSPTRPVPGNIRRPEYVGKPAPTP-YTGPE	(40)
6		--MSGQSLLVPGELSPTRSVPGNIRRPEYVGKPAPTP-YTGPE	(40)
7		MPA--RTALSPGFLSPTLPVPAWIPRPEYVGKPTAQEGS-ESW	(40)
8		MPA--RTALSPGALSPTLPVPARIPRPEYVGKPTAREGS-EPW	(40)
9	(4)	MSK-MRAPLVPGIPTPIREVPAHIERPEYVWKDEVQEAIGEPF	(42)
10		MAI-TREPLKPGHPTPIREVPAYIDRPEYVWKDEVQEAIGEPF	(42)
11		MSVRTRQPLVPGTPTPIREVPRSIERPEYAWKKTAKEGS-EPW	(42)

FIGURE 3: Sequence alignment of all known prokaryotic MetAPs with an N-terminal extension. These include (1) *Mycobacterium tuberculosis* (Q33343), (2) *Leifsonia xyli* (Q6AFH6), (3) *Tropheryma whipplei* (Q83GK8), (4) *Propionibacterium acnes* (Q6A9Z9), (5) *Streptomyces avermitilis* (Q82AX4), (6) *Streptomyces coelicolor* (Q9RKR2), (7) *Mycobacterium leprea* (Q9CBU7), (8) *Mycobacterium paratuberculosis* (Q73VS7), (9) *Corynebacterium glutamicum* (Q6M437), (10) *Corynebacterium diphtheria* (Q6NGLS), and (11) *Nocodia farcinica* (Q5YSA3). The identification codes for each of the proteins in the Swiss-prot/Tremble databases (*4*) are given in parentheses.

Presence of a Polyproline Motif. As early as 1971, Kerwar et al. (*29*) showed that methionine aminopeptidase in rat brain loosely associates with ribosomes. This is consistent with the idea that MetAPs might remove the N-terminal methionine as the polypeptide chain emerges from the site of synthesis. More recently, Vetro and Chang (*30*) showed directly that type I yeast MetAP binds to the 60S subunit and the 80S translational complex of the ribosome. On the basis of the properties of point and deletion mutants, they hypothesized that the zinc-finger domain at the N-terminus of yeast MetAP1 was important for the alignment of the protein on the ribosome. At the same time, the manner in which MetAPs interact with the ribosome has remained unclear. Several crystal structures of MetAPs with only the catalytic domain have been reported, but none has indicated the presence of a known protein- or RNA-recognition motif (*10*−*13*, *31*). This suggests that the ribosomal recognition sequence might be located in the N-terminal extension (Figure 1). However, no structure of a type Ib MetAP including this region has been described.

Even though the N-terminal extension of MtMetAP1c lies on the surface of the protein (Figure 2), its conformation is quite well-defined. Inspection of this region reveals that residues 14−17 have the sequence Pro-Thr-Arg-Pro. Furthermore, the conformation of this region appears to correspond to that of a polyproline II helix, that is, a left-handed helical structure with three residues per turn (*32*). This suggests that residues 14−17 of MtMetAP1c might correspond to a PxxP motif and, as such, be recognized by an SH3 domain. SH3−PxxP protein−protein interactions are known to play critical roles in assembly and in the regulation of many cellular signaling complexes (*33*). Binding affinity between PxxP peptides and SH3 domains is relatively weak ($K_D \sim 5-100\ \mu M$) (*34*) and in some cases is enhanced by contributions from other protein domains.

To test this idea further, we used model-building to determine whether a known SH3 domain could be aligned on the surface of MtMetAP1c. The NMR structure of the SH3 domain from Fyn proto-oncogene tyrosine kinase complexed with the synthetic peptide P2L (*35*) was used as a template. The result, shown in Figure 7a, is based on the superposition of prolines $P_{14}xxP_{17}$ of MtMetAP1c on prolines $P_{96}xxP_{99}$ of the peptide P2L. For the 14 aligned atoms within the two prolines, the rmsd was only 0.38 Å. Also, as shown in Figure 7b, the intervening residues have almost identical conformation. Thus $P_{14}xxP_{17}$ of MtMetAP1c does have the conformation of polyproline II. As can be seen in Figure 7b, aromatic residues from the SH3 domain fill the grooves formed by the PxxP motif. The overall alignment of the SH3 domain on MtMetAP1c, shown in Figure 7a, reveals no steric clash between the two molecules.

Interactions between MetAPs and the Ribosome. There is relatively little data on the mode of interaction between the MetAPs and the ribosome. As noted above, Kerwar et al. (*29*) showed an association between the MetAP in rat brain and the ribosome. The results did not indicate whether this interaction involves a type I or type II MetAP, or both.

Recently, it was shown that wild-type yeast MetAP1, as well as a mutant lacking residues 2−69 (Δ2−69), binds to both the 60S subunit and the 80S translational complex of

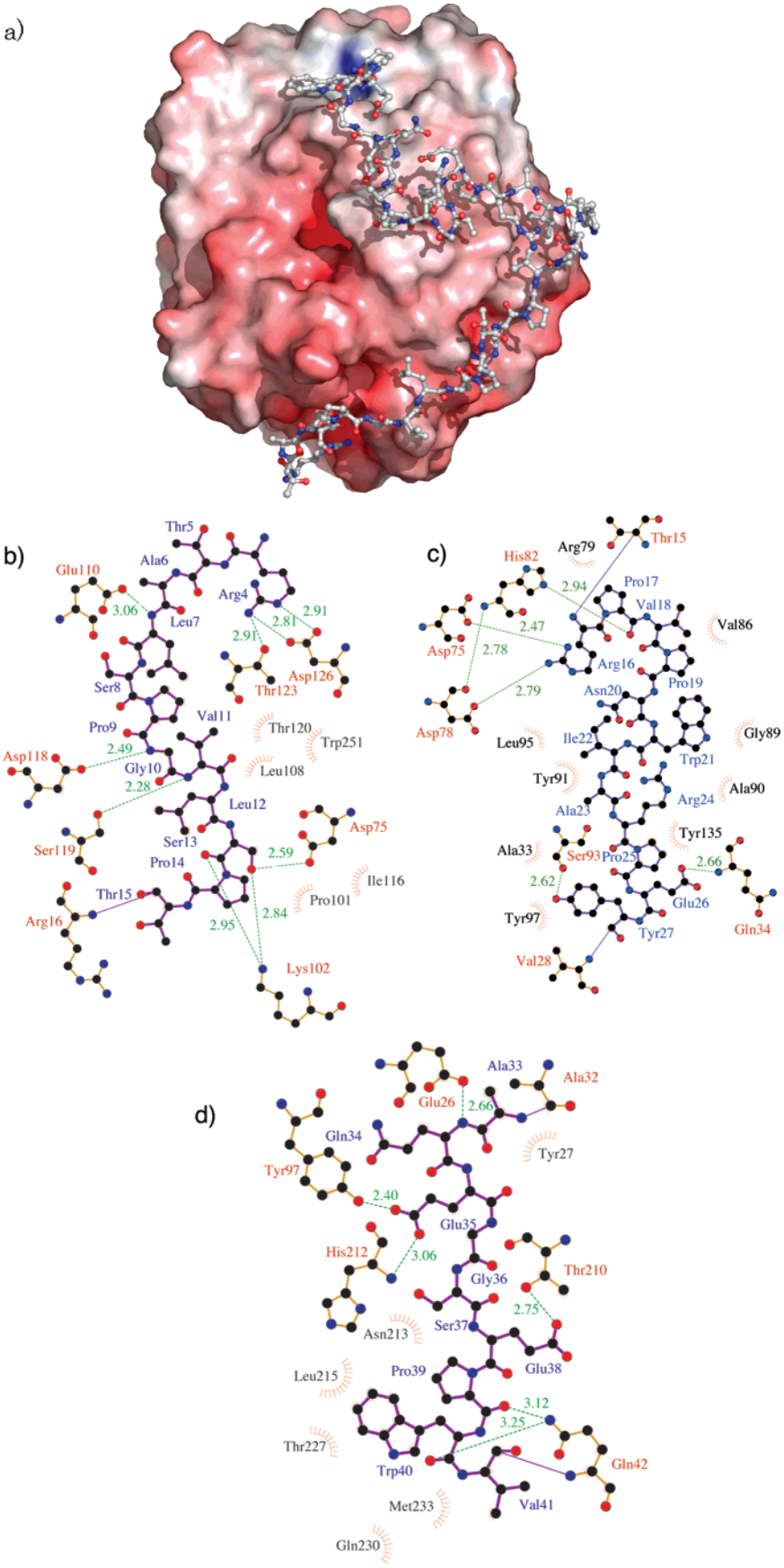

FIGURE 4: (a) Electrostatic surface potential of the catalytic domain of MtMetAP1c calculated without the N-terminal extension. Although not included in the calculation, the residues in the N-terminal extension are included in the figure. (b−d) Schematic diagrams showing the sequence-specific interactions between the catalytic domain and the N-terminal extension in MtMetAP1c. Atoms in the N-terminal extension are shown in magenta while those from the catalytic domain are shown in orange. The hatching illustrates a hydrophobic contact. (b) Residues 4−15. (c) Residues 16−27. (d) Residues 33−41. Panels b−d prepared with LIGPLOT (*43*).

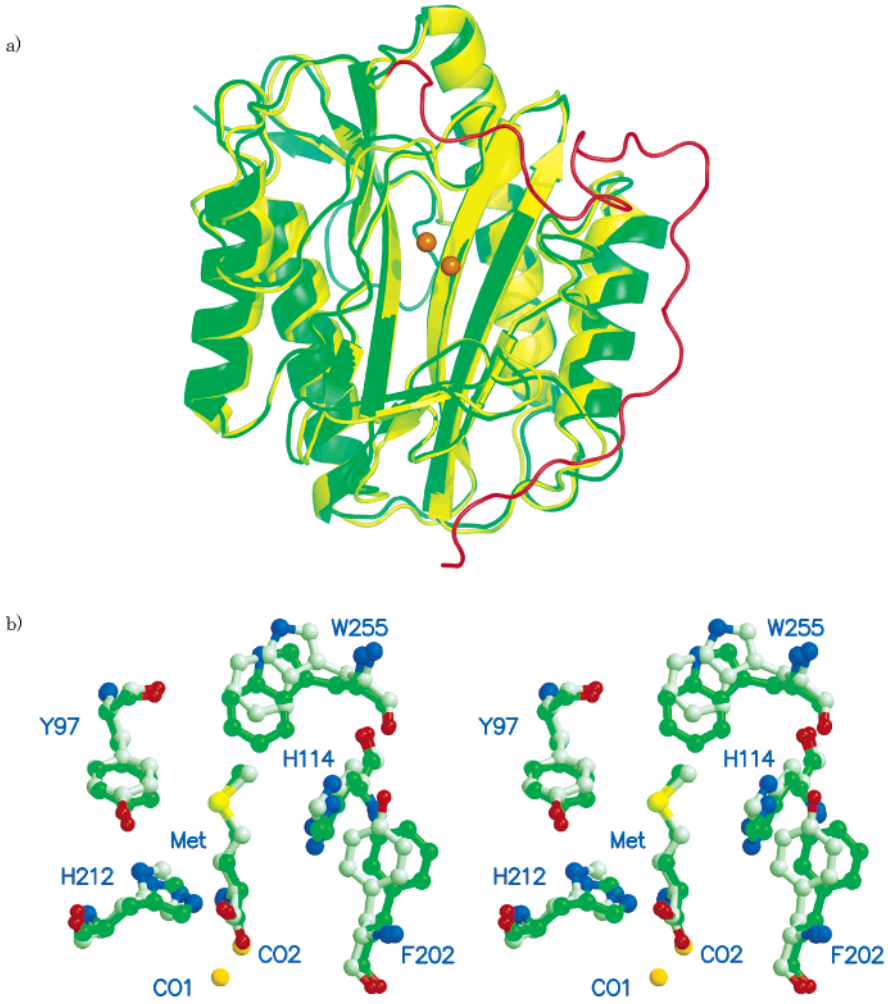

FIGURE 5: (a) The overlay of MtMetAP1c (yellow) and EcMetAP (green) shows that the overall shape of both proteins is very similar. The N-terminal extension of the MtMetAP1c is shown in red. (b) Stereo diagram comparing the complex of methionine with MtMetAP1c (green) and the complex of EcMetAP (PDB: 1C21) with methionine (gray).

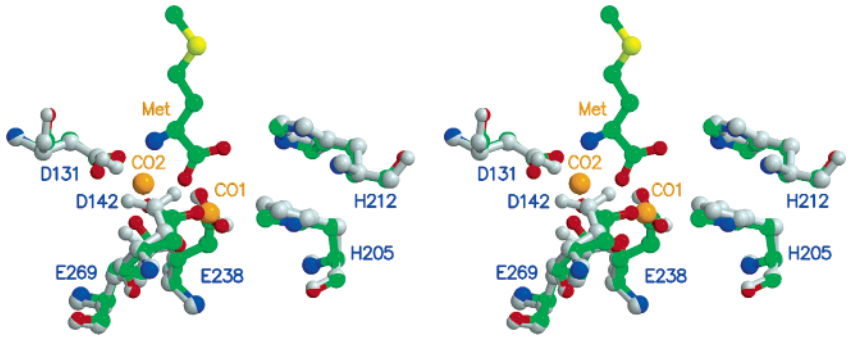

FIGURE 6: Stereoview comparing the active site of apo MtMetAP1c (gray) and the cobalt-enzyme in complex with methionine (in color). The main change is in the cobalt ligand Asp142.

the ribosome (*30*). At face value, this suggests that the site on the protein that binds to the ribosome is outside residues 2−69; that is, it does not include the zinc-finger domain. In conflict with this interpretation, however, the full-length protein with mutations C22S or H62R within the zinc-finger region was found to associate with the 40S rather than the 60S ribosomal subunit. This led Vetro and Chang (*5*) to suggest that the zinc-finger domain, which is essential for the normal processing function of MetAP1 in vivo, might help align MetAP1 on the ribosome. In vitro, there is no difference between the catalytic activity of the native protein, the Δ2−69 mutant, and the full-length protein containing the point mutants C22S and H62R. In vivo, however, these variants were less effective than wild-type in complementing a yeast *map1* null strain (*3*, *30*, *36*).

In summary, the experimental evidence for the location of a ribosome binding site within the MetAPs is not clear-cut, but the available data are consistent with a binding site within the linker region, as proposed in this work.

PxxP Motifs in Other Methionine Aminopeptidases. If ribosomes bind MetAPs by an interaction of an SH3 domain on the ribosome with a PxxP motif on MetAP, then PxxP

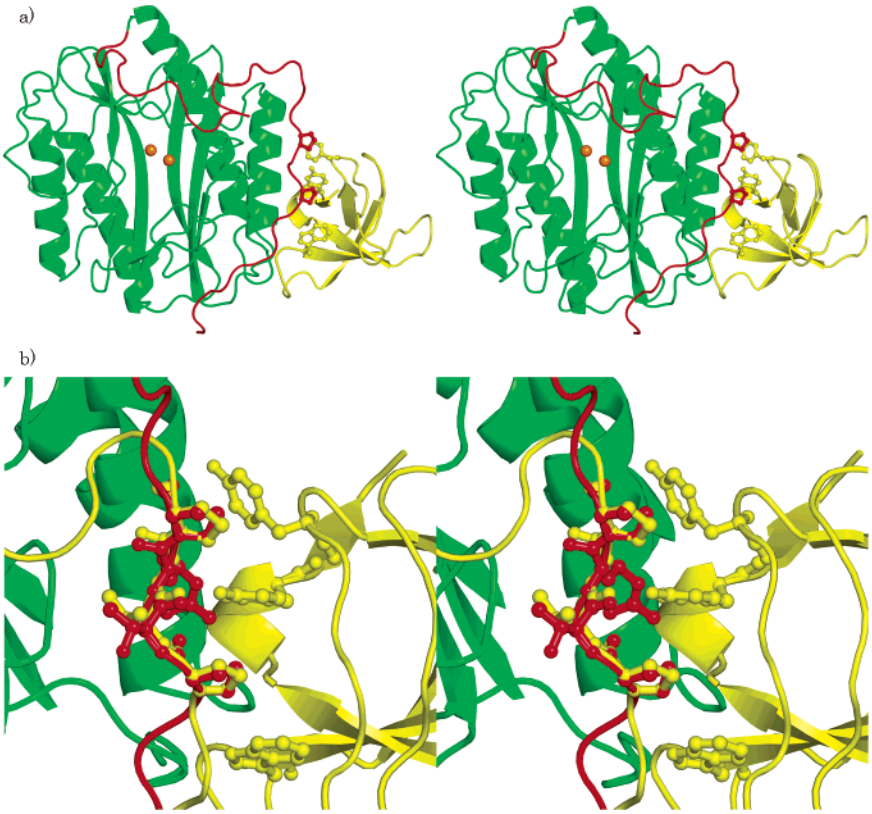

FIGURE 7: (a) Docking of the SH3 domain from Fyn proto-oncogene tyrosine kinase (shown in yellow) on *M. tuberculosis* MetAP1c (shown in green with the N-terminal extension in red). The two structures are aligned based on the superposition of prolines in the respective PxxP motifs [$P_{14}xxP_{17}$ in MetAP, and $P_{96}xxP_{99}$ in the P2L peptide complexed with the Fyn kinase[23]]. (b) Close-up showing the superposition of the PxxP motifs described in 3(a) ($P_{14}xxP_{17}$ of MetAP in red, $P_{96}xxP_{99}$ of the P2L peptide in yellow). The aromatic side chains in the Fyn kinase (shown in yellow) interdigitate with the prolines.

Human_75	T D P W A G Y R Y T G K L R P H Y P L M P T R P V P S Y I Q R P D Y A D H P L G M S E S E Q A L K G T S Q
Mouse_75	T D P W A G Y R Y T G K L R P H Y P L M P T R P V P S Y I Q R P D Y A D H P L G M S E S E Q A L K G T S Q
Zebrafish_68	T D P W P G Y R Y T G K L R P Y Y P L T P M R L V P S N I Q R P D Y A D H P L G M S E S E Q T M K G T S Q
Frog_75	T D P W P G Y R Y T G K L R P H Y P L T P M R P V P S Y I Q R P D Y A D H P L G M S E S E Q T L K G T S Q
Neurospora_63	Y N P F P T F S Y T G P L R P V Y P L S P K R V V P K S I P H P D Y A E S - - G I P G G G R - - T R S N K
Yeast_76	Y D P F P K F K Y S G K V K A S Y P L T P R R Y V P E D I P K P D W A A N - - G L P V S E Q R N D R L N N
Pest_82	Y N P W P Y Y T F T G K L R P - F E Q T P R R P V P P H I P R P D Y A D H K E G R S K S E E A L R G N N T
Fruitfly_64	Y N P W P H F R F T G K L R P - F P Q T P K R T V P N A I Q R P D Y A D H P A G R S L S E E A L R G T K -
Tuberculosis_1	- - - M P S - - - R T A L S P - G V L S P T R P V P N W I A R P E Y V G K P A A Q E G S E P W V Q T P E -

FIGURE 8: Sequences of eight representative type Ib eukaryotic MetAPs within the linker region (see Figure 1). The sequence of the N-terminal extension of *M. tuberculosis* MetAP1c is included for comparison. The number following the species is that of the starting residue [from InterPro, Mulder et al. (*25*)]. Prolines are shown in red. Residues shown in green appear at least six times among the total of nine sequences.

motifs should be a common feature of type Ib MetAPs. An inspection of the sequences of members of this family shows that this is indeed the case. Figure 8 shows an alignment of eight representative eukaryotic MetAP sequences in the vicinity of the linker between the zinc-finger region and the catalytic domain. Four of the eukaryotic sequences have a PxxP motif at the same location as in *M. tuberculosis*, and the other four have a PxxP sequence immediately preceding it (five of the eight have a repeated PxxPxxP motif). Of the 11 sequences identified for MetAP1c, nine have the PxxP sequence either in the same position or immediately preceding it (Figure 3). As can be seen in Figure 7b, the region of MetMetAP1c that corresponds to this proline-rich sequence has a polyproline II conformation and is located on the surface of the protein. Thus, either or both of the PxxP motifs in the eukaryotic MetAPs are suitably located to bind to an SH3 domain on the ribosome.

SH3 Domains within the Ribosome. A prediction of the proposed mode of interaction between type Ib MetAPs and the ribosome is that the ribosome should include an appropriately located SH3 domain. A search of the *InterPro* Web site (*37*), which categorizes protein domains based on sequence similarity with known structures, suggests that there are a number of ribosomal proteins that could have SH3 domains. These include eukaryotic initiation factor 5A, hypusine eIF-5A, and ribosomal proteins L2, L21e, and L24/L26.

Most of the known high-resolution ribosome structures are from prokaryotes. It had generally been thought that such prokaryotes would not contain SH3 domains, although recent studies suggest that this may not be the case (*38*−*40*). Inspection of the crystal structure of *Haloarcula marismortui* ribosome (*41*) shows that proteins L2, L21e, and L24 all have SH3 domains. In most cases, the SH3 domain is exposed on the surface of the ribosome. L24, in particular, is located adjacent to the tunnel where the nascent polypeptide chain emerges from the large subunit of the ribosome (Figure 9). This protein (L24) has sequence homology with the human ribosomal protein L26. This suggests that human type I MetAP bound to subunit L26 in the human ribosome would be suitably placed to cotranslationally remove an N-terminal methionine as it emerges from the ribosome.

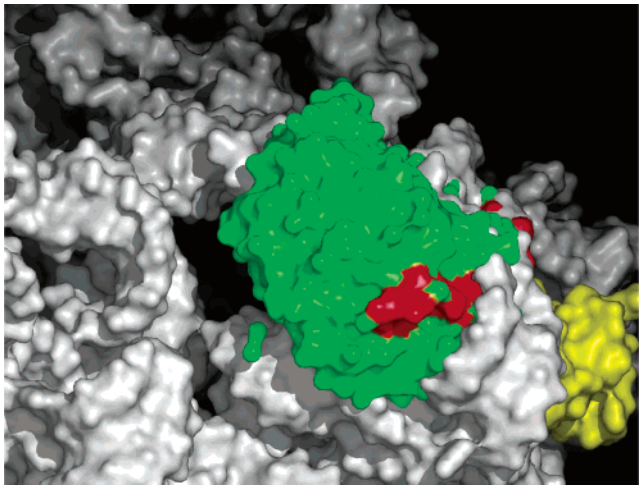

FIGURE 9: Space-filling model of the ribosome from *Haloarcula marismortui* (*40*) showing MetAP (green with N-terminal extension in red) aligned on subunit L24. Much of subunit L24 is obscured by the MetAP molecule, but part can still be seen (yellow). The exit channel for the nascent polypeptide chain is adjacent and to the left of the MetAP molecule and is shown in black.

Role of the N-Terminal Extension in Type Ic MetAPs. We have shown that the N-terminal extension in the type Ic MetAPs is highly conserved and is proline-rich. We have also shown that the PxxP motif in MtMetAPc is on the surface of the protein and appears geometrically poised to allow SH3 binding. We note that some MetAPs completely lack any N-terminal extension, suggesting that it does not play a role that is critical for all aspects of MetAP function. In the same context, it is not clear why some bacterial species have two MetAPs while others have only one. It is worth noting that the processing of newly synthesized polypeptides in bacteria is initiated by methionine deformylation (*42*). If a methionine aminopeptidase is to bind to the ribosome and remove the N-terminal methionine cotranslationally, then the deformylase must be either part of the overall complex or at least present in the vicinity. Answers to these questions will help to facilitate a better understanding of the process of N-terminal methionine removal during protein synthesis and its role in cell biology.

REFERENCES

1. Bradshaw, R. A., Brickey, W. W., and Walker, K. W. (1998) N-terminal processing: the methionine aminopeptidase and N alpha-acetyl transferase families, *Trends Biochem. Sci. 23*, 263−267.
2. Lowther, W. T., and Matthews, B. W. (2002) Metalloaminopeptidases: common functional themes in disparate structural surroundings, *Chem. Rev. 102*, 4581−4608.
3. Zuo, S., Guo, Q., Ling, C., and Chang, Y. H. (1995) Evidence that two zinc fingers in the methionine aminopeptidase from *Saccharomyces cerevisiae* are important for normal growth, *Mol. Gen. Genet. 246*, 247−253.
4. Boeckmann, B., Bairoch, A., Apweiler, R., Blatter, M.-C., Estreicher, A., Gasteiger, E., Martin, M. J., Michoud, K., O'Donovan, C., Phan, I., Pilbout, S., and Schneider, M. (2003) The SWISS-PROT protein knowledge base and its supplement TrEMBL in 2003, *Nucleic Acids Res. 31*, 365−370.
5. Li, X., and Chang, Y. H. (1995) Amino-terminal protein processing in *Saccharomyces cerevisiae* is an essential function that requires two distinct methionine aminopeptidases, *Proc. Natl. Acad. Sci. U.S.A. 96*, 12357−12361.
6. Chang, S. Y., McGary, E. C., and Chang, S. (1989) Methionine aminopeptidase gene of *Escherichia coli* is essential for cell growth, *J. Bacteriol. 171*, 4071−4072.
7. Liu, S., Widom, J., Kemp, C. W., Crews, C. M., and Clardy, J. (1998) Structure of human methionine aminopeptidase-2 complexed with fumagillin, *Science 282*, 1324−1327.
8. Lowther, W. T., McMillen, D. A., Orville, A. M., and Matthews, B. W. (1998) The anti-angiogenic agent fumagillin covalently modifies a conserved active-site histidine in the *Escherichia coli* methionine aminopeptidase, *Proc. Natl. Acad. Sci. U.S.A. 95*, 12153−12157.
9. Griffith, E. C., Su, Z., Niwayama, S., Ramsay, C. A., Chang, Y. H., and Liu, J. O. (1998) Molecular recognition of angiogenesis inhibitors fumagillin and ovalicin by methionine aminopeptidase 2, *Proc. Natl. Acad. Sci. U.S.A. 95*, 15183−15188.
10. Lowther, W. T., Orville, A. M., Madden, D. T., Lim, S., Rich, D. H., and Matthews, B. W. (1999) *Escherichia coli* methionine aminopeptidase: implications of crystallographic analyses of the native, mutant, and inhibited enzymes for the mechanism of catalysis, *Biochemistry 38*, 7678−7688.
11. Lowther, W. T., Zhang, Y., Sampson, P. B., Honek, J. F., and Matthews, B. W. (1999) Insights into the mechanism of *Escherichia coli* methionine aminopeptidase from the structural analysis of reaction products and phosphorus-based transition-state analogues, *Biochemistry 38*, 14810−14819.
12. Oefner, C., Douangamath, A., D'Arcy, A., Hafeli, S., Mareque, D., MacSweeney, A., Padilla, J., Pierau, S., Schulz, H., Thormann, M., Wadman, S., and Dale, G. E. (2003) The 1.15 Å crystal structure of the *Staphylococcus aureus* methionyl-aminopeptidase and complexes with triazole based inhibitors, *J. Mol. Biol. 332*, 13−21.
13. Douangamath, A., Dale, G. E., D'Arcy, A., Almstetter, M., Eckl, R., Frutos-Hoener, A., Henkel, B., Illgen, K., Nerdinger, S., Schulz, H., MacSweeney, A., Thormann, M., Treml, A., Pierau, S., Wadman, S., and Oefner, C. (2004) Crystal structures of *Staphylococcus aureus* methionine aminopeptidase complexed with keto heterocycle and aminoketone inhibitors reveal the formation of a tetrahedral intermediate, *J. Med. Chem. 47*, 1325−1328.
14. Ye, Q. Z., Xie, S. X., Huang, M., Huang, W. J., Lu, J. P., and Ma, Z. Q. (2004) Metalloform-selective inhibitors of *Escherichia coli* methionine aminopeptidase and X-ray structure of a Mn(II)-form enzyme complexed with an inhibitor, *J. Am. Chem. Soc. 126*, 13940−13941.
15. Stokstad, E. (2000) Infectious disease. Drug-resistant TB on the rise, *Science 287*, 2391.
16. Cole, S. T. (1994) *Mycobacterium tuberculosis*: drug-resistance mechanisms, *Trends Microbiol. 2*, 411−415.
17. Tsuyuguchi, I. (2001) Dialogue between *Mycobacterium tuberculosis* and *Homo sapiens*, *Tuberculosis 81*, 221−227.
18. Otwinowski, Z., and Minor, W. (1997) Processing of X-ray diffraction data collected in oscillation mode, *Methods Enzymol. 276*, 307−326.
19. Kissinger, C. R., Gehlhaar, D. K., and Fogel, D. B. (1999) Rapid automated molecular replacement by evolutionary search, *Acta Crystallogr. D55*, 484−491.
20. Brunger, A. T., Adams, P. D., Clore, G. M., DeLano, W. L., Gros, P., Grosse-Kunstleve, R. W., Jiang, J. S., Kuszewski, J., Nilges, M., Pannu, N. S., Read, R. J., Rice, L. M., Simonson, T., and Warren, G. L. (1998) Crystallography & NMR system: A new software suite for macromolecular structure determination, *Acta Crystallogr. D54*, 905−921.
21. Jones, T. A., Zou, J. Y., Cowan, S. W., and Kjeldgaard, M. (1991) Improved methods for building protein models in electron density maps and the location of errors in these models, *Acta Crystallogr. A47*, 110−119.
22. Chenna, R., Sugawara, H., Koike, T., Lopez, R., Gibson, T. J., Higgins, D. G., and Thompson, J. D. (2003) Multiple sequence alignment with the Clustal series of programs, *Nucleic Acids Res. 31*, 3497−3400.
23. Barton, G. J. (1993) ALSCRIPT: a tool to format multiple sequence alignments, *Protein Eng. 6*, 37−40.
24. Kleywegt, G. J., and Jones, T. A. (1997) Detecting folding motifs and similarities in protein structures, *Methods Enzymol. 255*, 525−545.
25. Kraulis, P. J. (1991) MOLSCRIPT: a program to produce both detailed and schematic plots of protein structures, *J. Appl. Crystallogr. 24*, 946−950.
26. DeLano, W. L. (2002) The PyMOL molecular graphics system, DeLano Scientific, San Carlos, CA.
27. Altschul S. F., Madden T. L., Schäffer A. A., Zhang J., Zhang Z., Miller W., and Lipman, D. J. (1997) Gapped BLAST and PSI-

BLAST: a new generation of protein database search programs, *Nucleic Acids Res. 25*, 3389−3402.
28. Li, J. Y., Chen, L. L., Cui, Y. M., Luo, Q. L., Gu, M., Nan, F. J., and Ye, Q. Z. (2004) Characterization of full length and truncated type I human methionine aminopeptidases expressed from *Escherichia coli*, *Biochemistry 43*, 7892−7898.
29. Kerwar, S. S., Weissbach, H., and Glenner, G. G. (1971) An aminopeptidase activity associated with brain ribosomes, *Arch. Biochem. Biophys. 143*, 336−337.
30. Vetro, J. A., and Chang, Y. H. (2002) Yeast methionine aminopeptidase type 1 is ribosome-associated and requires its N-terminal zinc finger domain for normal function in vivo, *J. Cell. Biochem. 85*, 678−688.
31. Roderick, S. L., and Matthews, B. W. (1993) Structure of the cobalt-dependent methionine aminopeptidase from *Escherichia coli*: a new type of proteolytic enzyme, *Biochemistry 32*, 3907−3912.
32. Mayer, B. J. (2001) SH3 domains: complexity in moderation, *J. Cell Sci. 114*, 1253−1263.
33. Zarrinpar, A., Bhattacharyya, R. P., and Lim, W. A. (2003) The structure and function of proline recognition domains, *Sci. STKE 2003*, RE8.
34. Dalgarno, D. C., Botfield, M. C., and Rickles, R. J. (1997) SH3 domains and drug design: ligands, structure, and biological function, *Biopolymers 43*, 383−400.
35. Renzoni, D. A., Pugh, D. J., Siligardi, G., Das, P., Morton, C. J., Rossie, C., Waterfield, M. D., Campbell, I. D., and Ladbury, J. E. (1996) Structural and thermodynamic characterization of the interaction of the SH3 domain from Fyn with the proline-rich binding site on the p85 subunit of PI3-kinase, *Biochemistry 35*, 15646−15653.
36. Dummitt, B., Fei, Y., and Chang, Y. H. (2002) Functional expression of human methionine aminopeptidase type 1 in *Saccharomyces cerevisiae*, *Protein Pept. Lett. 9*, 295−303.
37. Mulder, N. J., Apweiler, R., Attwood, T. K., Bairoch, A., Barrell, D., Bateman, A., Binns, D., Biswas, M., Bradley, P., Bork, P., Bucher, P., Copley, R. R., Courcelle, E., Das, U., Durbin, R., Falquet, L., Fleischmann, W., Griffiths-Jones, S., Haft, D., Harte, N., Hulo, N., Kahn, D., Kanapin, A., Krestyaninova, M., Lopez, R., Letunic, I., Lonsdale, D., Silventoinen, V., Orchard, S. E., Pagni, M., Peyruc, D., Ponting, C. P., Selengut, J. D., Servant, F., Sigrist, C. J. A., Vaughan, R., and Zdobnov, E. M. (2003) The InterPro database, 2003 brings increased coverage and new features, *Nucleic Acids Res. 31*, 315−318.
38. Nakagawa, A., Nakashima, T., Taniguchi, M., Hosaka, H., Kimura, M., and Tanaka, I. (1999) The three-dimensional structure of the RNA-binding domain of ribosomal protein L2; a protein at the peptidyl transferase center of the ribosome, *EMBO J. 18*, 1459−1467.
39. D'Aquino, J. A., and Ringe, D. (2003) Determinants of the Src homology domain, *J. Bacteriol. 185*, 4081−4086.
40. Yao, M., Ohsawa, A., Kikukawa, S., Tanaka, I., and Kimura, M. (2003) Crystal structure of hyperthermophilic archaeal initiation factor 5A: a homologue of eukaryotic initiation factor 5A (eIF-5A), *J. Biochem. 133*, 75−81.
41. Nissen, P., Hansen, J., Ban, N., Moore, P. B., and Steitz, T. A. (2000) The structural basis of ribosome activity in peptide bond synthesis, *Science 289*, 920−930.
42. Waller, J. P. (1963) The NH2-terminal residues of the proteins from cell-free extracts of *E. coli*, *J. Mol. Biol. 62*, 483−496.
43. Wallace, A. C., Laskowski, R. A., and Thornton, J. M. (1995) LIGPLOT: a program to generate schematic diagrams of protein−ligand interactions, *Protein Eng. 8*, 127−134.

BI0501176